

Is light neutralino as dark matter still viable?

Daniel T. Cumberbatch^{1 a}, Daniel E. López-Fogliani^{1,2 b}, Leszek Roszkowski^{1,3 c},
Roberto Ruiz de Austri^{4 d}, Yue-Lin S. Tsai^{1,3e}

¹*Department of Physics and Astronomy,
The University of Sheffield, Sheffield S3 7RH, England*

²*Laboratoire de Physique Théorique,
Université Paris-Sud, F-91405 Orsay, France*

³*The Andrzej Soltan Institute for Nuclear Studies, Warsaw, Poland*

⁴*Instituto de Física Corpuscular,
IFIC-UV/CSIC, Valencia, Spain*

Motivated by the recent re-confirmation by CoGENT of the low-energy excess of events observed last year, and the recent improved limits from the XENON-100 experiment that are in contention with the CoGENT data, we re-examine the low mass neutralino region of the Minimal Supersymmetric Standard Model and of the Next-to-Minimal Supersymmetric Standard Model, both without assuming gaugino mass unification. We make several focused scans for each model, determining conservative constraints on input parameters. We then determine how these constraints are made increasingly stringent as we re-invoke our experimental constraints involving the dark matter relic abundance, collider constraints from LEP and the Tevatron, and then from flavour physics, as a series of successive 2σ hard cuts. We find that for both models, when all relevant constraints are applied in this fashion, we do not generate neutralino LSPs that possess a spin-independent scattering cross section in excess of 10^{-5} pb and a mass $7 \text{ GeV} \lesssim m_\chi \lesssim 9 \text{ GeV}$ that is necessary in order to explain the CoGENT observations.

PACS numbers: 95.35.+d; LPT-Orsay 11/61

^a D.Cumberbatch@sheffield.ac.uk

^b daniel.lopez@th.u-psud.fr

^c L.Roszkowski@sheffield.ac.uk

^d rruiz@ific.uv.es

^e Sming.Tsai@fuw.edu.pl

I. INTRODUCTION

Recent data from several direct detection (DD) dark matter (DM) experiments have significantly heightened interests in the search and identification of the elusive DM, that is predicted to dominate the matter component of the Universe, in the form of weakly-interacting massive particles (WIMPs). These include the observations made by the CoGENT experiment [1], a p -type point contact Germanium detector, whose enhanced sensitivity, due to an unprecedented combination of target mass and reduced electronic noise, revealed a possible excess of low energy events [2] that has recently been re-affirmed in June 2011 [3]. If the exponential trend in these low recoil energy events is fully attributed to the elastic scattering of WIMP DM, then this signal is consistent with limits on the DM mass in the range $7 \text{ GeV} \lesssim m_{\text{DM}} \lesssim 9 \text{ GeV}$ and nucleon scattering cross section in the range $4 \times 10^{-41} \text{ cm}^2 \lesssim \sigma_N \lesssim 1.5 \times 10^{-40} \text{ cm}^2$, respectively [2, 3]. Remarkably, the CoGENT results favour a WIMP mass consistent with that indicated by the annual modulation count rate¹ measured by DAMA/LIBRA [4, 5], assuming elastic scattering and that σ_N is spin-independent (SI) [6–10].

However, the majority of the region in $m_{\text{DM}} - \sigma_N$ parameter space favoured by CoGENT appears to be in contention with recent results from direct detection experiments, in particular, those recently reported by XENON-100 [11], whose 2011 data consist of non-observations that appear to completely exclude the region favoured by CoGENT [12]. The CoGENT and DAMA/LIBRA results are also in contention with the recent observation of two “anomalous” events by CDMS-II [13, 14], although the discrepancies here are much less extensive than with XENON-100, and such events are not statistically significant enough to be able to claim a detection of DM (see, e.g., [15]). Some authors have previously concluded that the extent of the discrepancies between the results from CoGENT and DAMA and those from the other DD experiments may be partially reconciled by, for example, assuming a different proportion of elastic scattering events at DAMA/LIBRA that are channeled, adopting DM halo models (specifically pertaining to the escape velocity and velocity distribution of WIMPs), assuming a lower scintillation efficiency for Xenon, or assuming different couplings between WIMPs and either protons or neutrons (see e.g., [15] and references therein).

Motivated by past experimental findings, several authors have investigated the parameter space of various particle physics models capable of generating light WIMP DM candidates that may potentially explain the CoGENT and DAMA/LIBRA observations (see, e.g., [16–20]). However, many such investigations achieve this by conducting focused scans with finely-tuned parameters that result in points lying close to the CoGENT/DAMA favoured region, but provide a very poor fit to astrophysical and collider constraints.

In light of the recent release of the 2011 data from CoGENT and XENON-100, we follow a similar line and re-examine and directly compare the general behaviour of the neutralino low mass region of two popular particle physics models: the Minimal Supersymmetric Standard Model (MSSM) and the Next-to-Minimal Supersymmetric Standard Model (NMSSM). We select to investigate the NMSSM in addition to the popular MSSM since in the NMSSM we expect that a lower mass lightest supersymmetric particle (LSP) is more easily allowed, relative to that say in the MSSM, owing to the weakening of the LEP bounds on the Higgs mass and couplings to Standard Model (SM) particles due to its extended Higgs sector.

To conduct our investigation we use the nested sampling (NS) algorithm, implemented in the Bayesian interface tool **Multinest** [21], that is incorporated into the **SuperBayesS** [22] and **NMSPEC** [23] packages, to perform scans focused on the low neutralino mass region when imposing experimental constraints in the likelihood function. However, unlike other recent studies, we then also impose the same constraints on the parameter space via a series of (2σ) hard cuts on the resulting scan data. These hard cuts consist of an increasing number of constraints involving, firstly, those on the cosmological DM relic abundance, as inferred from cosmic microwave background (CMB) and galaxy cluster observations, secondly, from direct search limits inferred from particle colliders, e.g., LEP and the Tevatron, and, thirdly, from indirect constraints from flavour physics and the anomalous magnetic moment of the muon $(g - 2)_\mu$. For each set of hard cuts we highlight the parameter space for each of our models that is consistent with the limits on the LSP mass and SI nucleon scattering cross section that are imposed by DD limits.

The structure of this paper is as follows: In Sec. II we describe the details of the scanning procedure that we utilise to investigate the low mass sectors of our two particle physics models. In Sec. III we present and discuss the results of our scan of the MSSM obtained when imposing our three sets of constraints from (i) the DM relic density, (ii) collider physics (excluding flavour physics) and (iii) indirect limits (flavour physics and $(g - 2)_\mu$). In Sec. IV we present the results of our analogous scans on the NMSSM, and compare these results with those corresponding to the MSSM. Finally, in Sec. V we summarise our conclusions.

¹ In their June 2011 paper, CoGENT also claim to observe evidence of an annual modulation in their data that is consistent with the DAMA/LIBRA results [3].

II. OUR PROCEDURE

We are particularly interested in the light neutralino LSP region of a few GeV. Since this window is excluded in the usual MSSM by LEP constraints, we relax the assumption of gaugino mass unification. We do the same also in our study of the NMSSM, even though in this model a neutralino LSP can potentially evade LEP constraints more easily than that in the MSSM, and can therefore be much lighter, because of the possibility of a sizeable singlino component. We are particularly interested as to how light the neutralino LSP in the MSSM and the NMSSM can be and which experimental constraints dominate in defining the lower limit on its mass. Therefore, in this study we explore the low neutralino mass regions of both the MSSM and NMSSM, in each case by performing a single, focused NS scan over a wide range of input parameters.

In Table I we summarise the sets of experimental and theoretical constraints that we apply to our scans of the MSSM and NMSSM. In the top part of Table I we list the constraints relating to DM relic density and flavour physics that we invoke in the respective likelihood functions, using conventional Gaussian probability density functions (pdfs), as described in, e.g., [29]. The central part of Table I lists the collider constraints that we include in the MSSM likelihood function, again using a Gaussian approximation, associated with our corresponding scan. The exception to this is the constraint on the mass of the pseudoscalar Higgs m_A which takes the form of a non-trivial function $f(m_{h_1})$ (with a corresponding inverse function $g(m_A)$) of the lightest CP-even Higgs mass m_{h_1} (and $\tan\beta$); see, e.g., [28] for further details. We approximate this constraint in our initial scan by invoking the constraint $m_{h_1} > 89$ GeV in the likelihood using a half-Gaussian approximation (we then later invoke the full functional constraints given by $f(m_{h_1})$ and $g(m_A)$ as a 2σ hard cut; see below). We also invoke all relevant collider constraints in the NMSSM likelihood function during our respective scan. These constraints, which are specified in the `NMSSMTool` code, are applied in our scan only as 2σ hard cuts in the relevant likelihood function due to computational challenges. Because of the complicated process in which collider constraints are invoked in the NMSSM we omit them in Table I and instead refer the reader to [23] for further details. Finally, the bottom part of Table I lists the nuisance parameters, and their corresponding ranges of values, over which we perform our scans. Unless otherwise stated, all ranges of values provided in Table I

Category	Experimental constraint	Reference
DM relic density	$\Omega_\chi h^2 = 0.1123 \pm 0.0035$ (expt) $\pm 0.1 \Omega_\chi h^2$ (th)	[24]
Flavour physics	$BR(B \rightarrow X_s \gamma)/10^{-4} = 3.55 \pm 0.26$ (expt) ± 0.21 (th)	[25]
	$BR(B_u \rightarrow \tau \nu_\tau)/10^{-4} = 1.41 \pm 0.43$ (expt) ± 0.38 (th)	[26]
	$BR(\bar{B}_s \rightarrow \mu^+ \mu^-) < 5.8 \times 10^{-8}$ (95% C.L.)	[26]
	$\delta(g-2)_\mu/10^{-10} = 29.5 \pm 8.8$ (expt) ± 1 (th)	[26]
Collider (MSSM only)	$\Gamma_{\text{inv}} = 499 \pm 1.5$ MeV	[27]
	$m_{\chi_1^\pm} > 94$ GeV (95% C.L.)	[27]
	$m_{h_1} = g(m_A)$ (2σ hard cut only)	[28]
	$m_{\tilde{e}_R} > 73$ GeV (95% C.L.)	[27]
	$m_{\tilde{\mu}_R} > 94$ GeV (95% C.L.)	[27]
	$m_{\tilde{\tau}_1} > 81.9$ GeV (95% C.L.)	[27]
	$m_A = f(m_{h_1})$ (2σ hard cut only)	[28]
Collider (NMSSM only)	As implemented in <code>NMSSMTools</code> .	[23]
Nuisance parameters	$M_t = 171.4 \pm 2.1$ GeV (expt)	[27]
	$m_b(m_b)^{\overline{MS}} = 4.20 \pm 0.07$ GeV (expt)	[27]
	$\alpha_s(M_Z)^{\overline{MS}} = 0.1176 \pm 0.002$ (expt)	[27]
	$1/\alpha_{\text{em}}(M_Z)^{\overline{MS}} = 127.955 \pm 0.018$ (expt) (MSSM only)	[27]

TABLE I. *Top*: a list of experimental constraints relating to DM relic density and flavour physics that are invoked in the respective likelihood functions, using a Gaussian approximation, associated with our scans of the MSSM and NMSSM. *Centre*: a list of collider constraints that are invoked into the likelihood function, using a Gaussian approximation [29], associated with our scan of the MSSM. The exception to this is the constraint on m_A and m_h , which we approximate in the likelihood via a half-Gaussian corresponding to $m_{h_1} > 89$ GeV. Then, later, as we do for all other collider constraints, we invoke the constraints given by $f(m_{h_1})$ and $g(m_A)$ as a 2σ hard cut on the points selected by our initial scan. The collider constraints invoked in our corresponding scan of the NMSSM are invoked as hard cuts in the respective likelihood function. The procedure in which collider constraints are invoked in our scan of the NMSSM via the `NMSSMTool` code is significantly more complex than that which we adopt for the MSSM, and we refer the reader to [23] for further details. *Bottom*: a list of the nuisance parameters, and their corresponding ranges of values, over which our scans are performed. Unless otherwise stated, all ranges of values provided are displayed along with their corresponding 1σ experimental (expt) and, where indicated, theoretical (th) errors.

are displayed along with their corresponding 1σ experimental (expt) and, where indicated, theoretical (th) errors. Following our initial NS scans we then successively apply hard cuts to the results using the respective 2σ ranges of specified combinations of the invoked constraints, where in the case of m_A and m_{h_1} we invoke the constraints given by $f(m_{h_1})$ and $g(m_A)$ as a 2σ hard cut.

An alternative to the above strategy would be to perform three separate scans over both MSSM and NMSSM input parameters, omitting subsequent hard cuts, where in each case using a likelihood function invoked with a successively increasing number of experimental constraints, i.e., ‘likelihood(DM relic density)’, ‘likelihood(DM relic density+collider)’, and ‘likelihood(DM relic density+collider+flavour)’. Despite the efficient nature of such scans, this strategy possesses two problems. Firstly, using these three different likelihood functions to investigate the low mass neutralino regime can result in posterior pdfs centred upon very different regions of parameter space. For example, it is quite possible that the favoured regions resulting from the ‘likelihood(DM relic density+collider)’ scan will not significantly overlap with that from the ‘likelihood(DM relic density)’ scan, making statistical arguments regarding the overall favoured region difficult. Secondly, if we include all experimental constraints into the likelihood function, the resulting χ^2 , which, given our assumptions and priors, is given by $-2\log[\text{likelihood}]$, can be written as

$$\chi_{\text{tot}}^2 = \chi_1^2 + \chi_2^2 + \dots, \quad (1)$$

where χ_i^2 represents the χ^2 statistics associated with a particular experimental constraint. In NS scans, Eq. (1) allows for, and often results in, points being selected which predict values that satisfy some constraints extremely well but lie far outside of the usual 1σ range of others, often used in traditional fixed-grid scans, whilst still yielding acceptable χ_{tot}^2 values. Moreover, such a method lacks transparency as to how the results of its scans correspond with individual experimental constraints.

Since in our scans we apply all experimental constraints as Gaussians in the likelihood functions (with the exception being those on m_A and m_h ; see above), and subsequently make 2σ cuts on the corresponding results, we are hence able to overcome both of the above issues. However, we emphasise that, because of this we will not provide a statistical interpretation of the point distribution of our numerical scans and display all our results as scatter plots, illustrating only the density of points, rather than pdfs. We use the NS scanning technique effectively to take advantage of the fact that it can perform an efficient scan of a multi-dimensional parameter space in order to obtain a representative sample of points, for specified ranges of parameters, allowing us to simply observe the general behaviour of this parameter space, rather than to draw statistical conclusions from our scans.

III. RESULTS IN THE MSSM

In this section, our goal is to map out the mass range of the light neutralino LSP in the MSSM that is consistent with current estimates for the present dark matter relic abundance, as well as constraints, both direct and indirect, from collider experiments. It is clear that because existing experimental limits are so stringent, especially those from LEP regarding the chargino mass, one needs to consider scenarios that have the potential to evade them in order to explore the low mass regime in which we are interested. On the other hand, in order to conduct a numerical scan that is manageable, one needs to focus primarily upon the parameters which are relevant to the problem at hand.

Bearing this in mind, we assume minimal flavour violation and perform a scan, as described in Sec. II, over the following MSSM parameters:

$$M_1, M_2, \mu, \tan \beta, m_A, m_{\tilde{l}_L}, m_{\tilde{l}_R}, \quad (2)$$

where M_1 and M_2 are the soft bino and wino masses respectively, μ is the Higgs/higgsino mass parameter, $\tan \beta$ is the ratio of the vacuum expectation values (VEVs) of the up and down-type neutral Higgs fields, m_A is the mass of the pseudoscalar Higgs boson, whilst $m_{\tilde{l}_L}$ and $m_{\tilde{l}_R}$ are the left and right hand slepton soft mass parameters. (For a more detailed description of the MSSM, we refer the reader to a dedicated review, e.g., [30].) We adopt log priors for all mass input parameters, and a flat prior for $\tan \beta$. The prior ranges of the MSSM parameters over which our scan is performed are provided in Table II.

We take all left-handed slepton soft mass parameters to be family degenerate (i.e., $m_{\tilde{e}_L} = m_{\tilde{\mu}_L} = m_{\tilde{\tau}_L} = m_{\tilde{l}_L}$), and likewise for their right-handed partners. On the other hand, gluino and squark masses will not play any significant role in determining either the relic density $\Omega_\chi h^2$ or the spin-independent elastic scattering cross section σ_p^{SI} , and hence we fix them at 1 TeV. Likewise, we fix all the trilinear couplings at the electroweak (EW) scale: $A_t = A_b = A_\tau = \tilde{A} = -0.5$ TeV. In order to focus our scan towards the low mass region of a few GeV, we adopt a log prior distribution of the bino mass M_1 , which primarily determines the mass, m_χ , of the lightest neutralino. Also we note that allowing for a more generous range of parameters by expanding the lower limits beyond those displayed would result in our scan

Parameter	Range	Parameter	Range
bino mass	$0.1 < M_1 < 40$	pseudoscalar mass	$85 < m_A < 600$
wino mass	$90 < M_2 < 150$	slepton-left mass	$70 < m_{\tilde{l}_L} < 3000$
μ parameter	$90 < \mu < 150$	slepton-right mass	$70 < m_{\tilde{l}_R} < 3000$
ratio of Higgs doublet VEVs	$1 < \tan \beta < 62$		

TABLE II. The prior ranges of input parameters over which we perform our scan of the MSSM. All displayed mass ranges are given in GeV. We adopt log priors for all mass input parameters, and a flat prior for $\tan \beta$

finding a disproportionate number of points in the region inconsistent with collider constraints. Note that, because we relax the usual assumption of gaugino mass unification (i.e., $M_3 : M_2 : M_1 \simeq 6 : 2 : 1$), and take the prior range of M_1 well below those of M_2 and of μ , in order to more efficiently generate light, bino-like neutralino LSP that can evade LEP constraints on the invisible Z width and the chargino mass [15]. Another parameter that will play an important role in our scan is $\tan \beta$ since it affects both m_χ as well as the fermion-sfermion couplings of the neutralino LSP, especially in the low mass regime that we are interested in, and we take a very wide range of its values in our scans.

To start with, in the left panel of Fig. 1 we present the results of our MSSM scan in the $m_\chi - \Omega_\chi h^2$ plane. Grey points denote all the points resulting from our NS scan, where constraints on $\Omega_\chi h^2$, collider limits and flavour physics constraints, as specified in Table I, are included in the likelihood. Since we display our results in the $m_\chi - \Omega_\chi h^2$ plane we of course omit any hard cuts on the relic abundance, but instead simply illustrate the corresponding 2σ range (dashed lines).

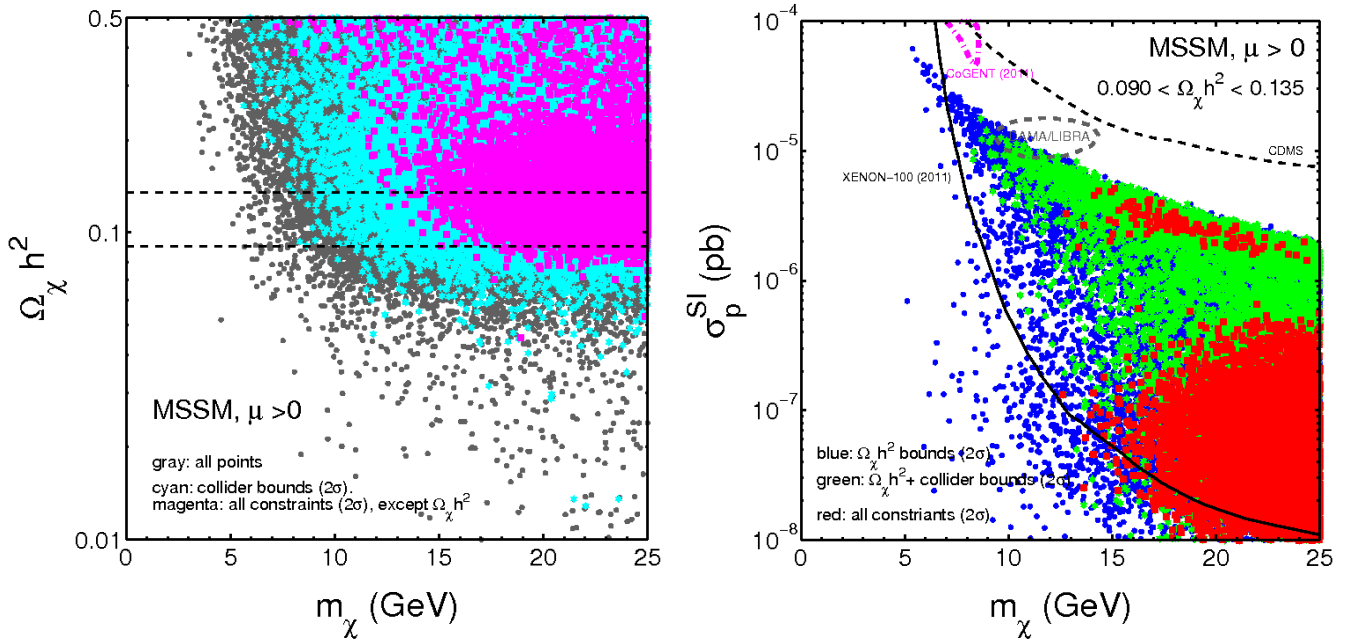


FIG. 1. *Left panel:* m_χ vs. $\Omega_\chi h^2$ in the MSSM. Grey points: all the points resulting from our NS scan, where constraints on $\Omega_\chi h^2$, collider limits and flavour physics constraints, as specified in Table I, are included in the likelihood. Cyan points: points from our scan surviving subsequent 2σ hard cuts using collider bounds. Magenta points: points from our scan surviving subsequent 2σ hard cuts using both collider and flavour physics constraints. We also indicate the 2σ range of relic densities within the experimental best-fit value (black dashed curves). *Right panel:* m_χ vs. σ_p^{SI} in the MSSM. Blue points: configurations in our initial NS scan yielding relic densities in the range: $0.090 < \Omega_\chi h^2 < 0.135$ (i.e., 2σ range). Green points: points that survive a 2σ hard cut using both relic density and collider bounds. Red points: MSSM parameter configurations surviving 2σ hard cuts using all constraints listed in Table I. We note that the results corresponding to $\Omega_\chi h^2 \leq \Omega_{\text{DM}} h^2$ are very similar to those displayed in this panel following our hard cuts, with only a handful of additional points being found in the region: $m_\chi \gtrsim 10$ GeV, $\sigma_p^{\text{SI}} \lesssim 2 \times 10^{-5}$ pb. We also illustrate the regions of parameter space currently favoured by the CoGENT (outlined by the magenta dash-dotted curve) and DAMA/LIBRA (with ion channelling, outlined by the dashed grey curve) experiments, and display the current limits from CDMS-II (dashed black curve) and XENON-100 (solid black curve).

Some features are clearly visible. Firstly, we observe a great number of points that predict a relic density that far exceeds the corresponding 2σ upper limit, particularly those in the low m_χ region. However, we also observe that there are points in this region that predict a relic density within the 2σ limits indicated by the black dashed curves. This is predominantly achieved through efficient t -channel annihilations via light stau exchange, where the $\chi\tau\tilde{\tau}_R$ coupling, which scales as $\tan^2\beta$, and hence, is enhanced at large $\tan\beta$. In fact, we find no points with $\tan\beta < 4$ for $m_\chi < 35$ GeV that predict a relic density within the experimental 2σ range. This result is simply a reflection of the SUSY neutralino equivalent of the Lee-Weinberg bound on massive neutrinos [31]. By requiring $\Omega_\chi h^2$ to be within the 2σ range, we find $m_\chi \gtrsim 5$ GeV, which is indeed consistent with the results previously obtained in [19]. Such low mass points appear to be absent in Fig. 3 of [18], which finds $m_\chi \gtrsim 11$ GeV, although, since cuts were made at the 68% C.L., it is possible that points possessing smaller m_χ but poorer likelihood were generated there.

Unfortunately, obtaining points with the desired small values of m_χ of a few GeV comes at the expense of potentially grossly violating other constraints, as mentioned in Sec. II. In order to see this, we impose a hard cut of 2σ on all of the collider constraints listed in Table I. The points surviving this cut are displayed in the left panel of Fig. 1 in cyan. We can clearly observe that a sizeable number of the points found in our scan (i.e. grey points), especially predicting low m_χ and/or low $\Omega_\chi h^2$, badly violate collider limits. We also find that, because of the strong correlation between the lower limit on m_χ and the minimum slepton mass, invoking the LEP constraint on $m_{\tilde{e}_R}$, $m_{\tilde{\mu}_R}$ and $m_{\tilde{\tau}_1}$ are responsible for the observed increase in the lowest value of m_χ possessed by a point generated from our scan that satisfies the 2σ bounds on $\Omega_\chi h^2$ from roughly 5 GeV (for the grey points in the left panel of Fig. 1) to approximately 7 GeV when LEP constraints are invoked (corresponding to the cyan points in the left panel of Fig. 1). Finally, we impose the remaining constraints from flavour physics and the anomalous magnetic moment of the muon, once again by making a 2σ hard cut on the initial set of points selected in our NS scan. The surviving points are shown in the left panel of Fig. 1 in magenta.

Following the above sets of hard cuts we can clearly observe that whilst the LSP with mass as small as 5 GeV still survives, which may lie within the range of WIMP mass favoured by CoGENT and DAMA/LIBRA (with ion channelling; see, e.g., [9]), only points with $m_\chi \gtrsim 13$ GeV, which lie outside of the ranges favoured by these experiments, predict values of $\Omega_\chi h^2$ consistent with the corresponding 2σ constraint.

In the right panel of Fig. 1 we demonstrate, this time in the m_χ - σ_p^{SI} plane, the effect of applying an increasing number of our constraints. The blue points represent the configurations in our initial NS scan that yield a value of $\Omega_\chi h^2$ within the favoured 2σ range $0.090 < \Omega_\chi h^2 < 0.135$. The green points illustrate those of the blue points that survive a 2σ hard cut using collider bounds. Finally, the red points correspond to those MSSM parameter configurations that survive hard cuts using all of the constraints in Table I, imposed at 2σ .

We note that we also conducted separate scans, identical to those described above except that the neutralino LSP generated was allowed to contribute only *partially* to the currently inferred DM abundance by invoking a 2σ upper bound of $\Omega_\chi h^2 < 0.135$ in the likelihood function. The results we found were very similar to those displayed in the right panel of Fig. 1, with only a handful of additional points being found in the region: $m_\chi \gtrsim 10$ GeV, $\sigma_p^{\text{SI}} \lesssim 2 \times 10^{-5}$ pb. The robustness of our results with respect to the constraints on $\Omega_\chi h^2$ is consistent with the findings of Vasquez *et al.* [18]. However we also note that whilst in [18] it was claimed that neutralino mass should obey $m_\chi \gtrsim 28$ GeV in order to evade present experimental bounds, determined primarily by the limits from XENON-100 (see Fig. 7 of [18]), from Fig. 1 (right panel) we find points with m_χ as small as $\simeq 13$ GeV that satisfy both the XENON-100 limits as well as our additional 2σ hard cuts.

In the MSSM the SI elastic scattering cross section σ_p^{SI} is primarily determined by the t -channel exchange of the heavy Higgs scalar H , with the effective $\chi H p$ coupling being enhanced by large values of $\tan\beta$. However, because of LEP bounds on the Higgs sector, in the MSSM, one is left with little freedom to boost σ_p^{SI} towards the regions currently favoured by CoGENT and DAMA/LIBRA (with ion channelling), as outlined in Fig. 1 by the magenta dash-dotted curve and the dashed grey curve respectively. Moreover, even for the blue points in Fig. 1 (right panel), where only a 2σ hard cut on $\Omega_\chi h^2$ is performed, the Higgs mass is not entirely unrestricted because of the lower limits of our selected prior ranges for MSSM input parameters (see Table II). We can also see that imposing collider bounds has the substantial effect of cutting off the wedge of points with $m_\chi \lesssim 8$ GeV possessing the largest SI elastic scattering cross sections, $\sigma_p^{\text{SI}} \gtrsim 2 \times 10^{-5}$ pb, which lie just below the CoGENT favoured region. On the other hand, we note that collider constraints have a fairly limited effect at larger values of m_χ .

In Fig. 1 (right panel), we observe that when we impose our 2σ hard cuts using collider and flavour physics constraints a vast number of points in the region: $m_\chi \lesssim 13$ GeV, $\sigma_p^{\text{SI}} \gtrsim 3 \times 10^{-6}$ pb are excluded. Such points are consistent with those found in the fore-mentioned investigation of the MSSM in [19] for $85 \text{ GeV} \lesssim m_A \lesssim 100 \text{ GeV}$ and $\tan\beta \gtrsim 30$. However, as remarked above, when we invoke flavour physics constraints, particularly those on $BR(\overline{B} \rightarrow X_s \gamma)$ (and also $BR(\overline{B}_s \rightarrow \mu^+ \mu^-)$, see below), as 2σ hard cuts, such points are clearly excluded. To confirm this, we note that we performed a separate scan of the MSSM, focused on the range of m_A and $\tan\beta$ mentioned above and using values of the input parameters that range over those utilised in [19]. We found that the resulting points possessed

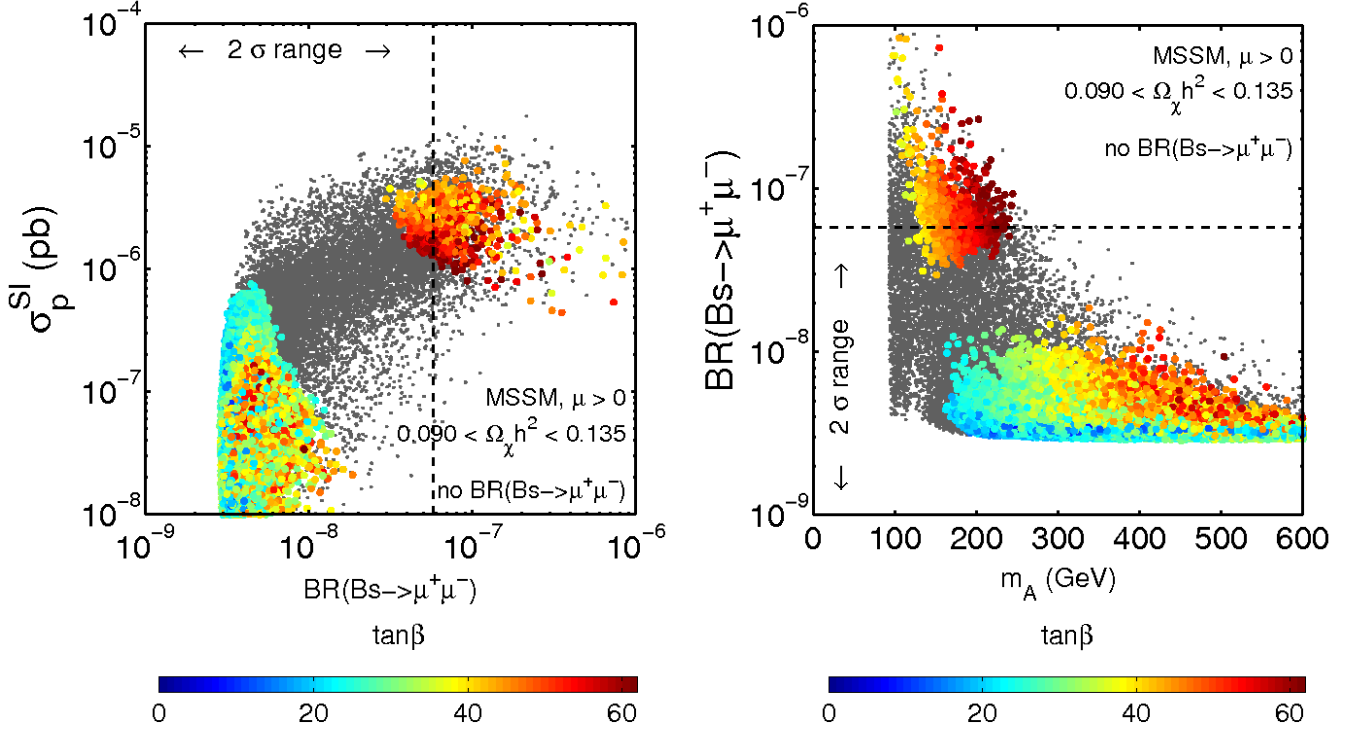


FIG. 2. *Left panel:* $BR(\overline{B}_s \rightarrow \mu^+ \mu^-)$ vs. σ_p^{SI} in the MSSM. Grey points: points from our initial NS scan which survive subsequent 2σ hard cuts using both our $\Omega_\chi h^2$ and collider constraints. Coloured points: those of the grey points which survive 2σ hard cuts using our flavour physics constraints, excluding that on $BR(\overline{B}_s \rightarrow \mu^+ \mu^-)$. The colour scale denotes the value of $\tan\beta$ associated with each point. We also illustrate the Tevatron limit on $BR(\overline{B}_s \rightarrow \mu^+ \mu^-)$ (dashed line). *Right panel:* m_A vs. $BR(\overline{B}_s \rightarrow \mu^+ \mu^-)$ in the MSSM, using the same colour scale as displayed in the left panel.

$BR(\overline{B} \rightarrow X_s \gamma) > 4.31 \times 10^{-4}$ (i.e., 2.3σ result) and hence, from Table I, fail to survive our 2σ hard cuts, confirming the results from our larger scans.

Upon further examination, we find that it is fairly easy to generate points that satisfy the constraints imposed on $BR(\overline{B} \rightarrow X_s \gamma)$, $BR(B_u \rightarrow \tau \nu_\tau)$, as well as on $\delta(g-2)_\mu$. In particular, the latter constraint is especially weak since, in order to generate a large enough SUSY contribution to the relic density, one requires a fairly light smuon, which, being a free parameter, is easy to produce, which in turn can give a substantial contribution to $\delta(g-2)_\mu$.

On the other hand, an improved upper bound on $BR(\overline{B}_s \rightarrow \mu^+ \mu^-)$ from the Tevatron puts a rather strong limit on the upper range of σ_p^{SI} values generated in our scan. This can be seen in the left panel of Fig. 2, where we plot the values of $BR(\overline{B}_s \rightarrow \mu^+ \mu^-)$ against σ_p^{SI} generated by some of the points in our initial NS scan. Grey points represent those scan points which survive subsequent 2σ hard cuts using both our DM and collider constraints, while the coloured points represent those of the grey points which survive further 2σ hard cuts using flavour physics constraints, except for that on $BR(\overline{B}_s \rightarrow \mu^+ \mu^-)$. From Fig. 2 we also observe the well-known correlation between σ_p^{SI} and $BR(\overline{B}_s \rightarrow \mu^+ \mu^-)$, arising from the fact that $BR(\overline{B}_s \rightarrow \mu^+ \mu^-) \propto \tan^6 \beta / m_A^4$ and that $m_A \simeq m_H$ for $m_A \gg 100$ GeV [32, 33]. On the other hand, at smaller m_A (~ 100 GeV) this correlation is relaxed because the approximate mass degeneracy does not hold there.

In Fig. 2 (left panel) we observe two “islands” of points. The one in the bottom left corner is constituted by points possessing low to average values of $\tan\beta$, which survive the upper limit on $BR(\overline{B}_s \rightarrow \mu^+ \mu^-)$ from the Tevatron, but produce values of $\sigma_p^{\text{SI}} \lesssim 10^{-6}$ pb, much smaller than those favoured by CoGENT or DAMA/LIBRA (with ion channelling). On the other hand, points constituting the upper right-hand island generate values of σ_p^{SI} up to $\sim 10^{-5}$ pb, that include the handful of red points located in the region: $10^{-6} \lesssim \sigma_p^{\text{SI}} \lesssim 6 \times 10^{-6}$ pb, $m_\chi \gtrsim 13$ GeV, but are mostly in conflict with the upper limit on $BR(\overline{B}_s \rightarrow \mu^+ \mu^-)$. Such points possess large values of $\tan\beta$ and also small values of m_A , reaching very close to the corresponding LEP limits for the MSSM, worsening their overall likelihood [27, 28]. This can be seen from the right panel of Fig. 2, where we plot the values of m_A against the values of $BR(\overline{B}_s \rightarrow \mu^+ \mu^-)$ possessed by the same points as displayed in the left panel. A more thorough treatment of Higgs LEP limits by including them in the likelihood could possibly produce more points with a larger σ_p^{SI} but again they

would likely correspond to stretching the LEP limits.

From Fig. 2 it is clear that in the MSSM, the effect of imposing all the relevant constraints as hard cuts, especially that on $BR(\overline{B}_s \rightarrow \mu^+ \mu^-)$, even at the somewhat relaxed level of 2σ , is to exclude any of our points located in either of the regions favoured by CoGENT or DAMA/LIBRA (with ion channelling). However, as remarked in Sec. I, we note that some authors (see, e.g., [15] and references therein) have illustrated how these favoured regions may be shifted slightly when taking into account certain uncertainties relating to the velocity distribution of Galactic DM or the detectors themselves.

IV. RESULTS IN THE NMSSM

In this section, we continue our discussion of the low mass neutralino region, now turning to our analysis of the NMSSM, starting briefly with a summary of some basic properties of the NMSSM. For a more detailed description of the NMSSM we refer the reader to a dedicated review (see, e.g., [34]).

A. The NMSSM

The NMSSM is an extension of the MSSM that provides a solution to the so-called μ -problem [35]. Its superpotential differs to that of the MSSM in that it contains a new superfield S which is a singlet under the SM gauge group $SU(3)_c \times SU(2)_L \times U(1)_Y$. (We use the same notation for superfields and their respective spin-0 component fields for simplicity.) The part of the NMSSM superpotential involving Higgs fields is given by

$$W = -\epsilon_{ij} \lambda S H_d^i H_u^j + \frac{1}{3} \kappa S^3, \quad (3)$$

where $H_d^T = (H_d^0, H_d^-)$, $H_u^T = (H_u^+, H_u^0)$, i, j are $SU(2)$ indices with $\epsilon_{12} = -1$, while λ and κ are dimensionless couplings in the extended Higgs sector. The superpotential Eq. (3) is scale invariant, and the EW scale will only appear through the corresponding soft SUSY breaking terms in the soft Lagrangian, $\mathcal{L}_{\text{soft}}$. Using the above notational conventions, the terms in $\mathcal{L}_{\text{soft}}$ associated with Eq. (3) are given by

$$\begin{aligned} -\mathcal{L}_{\text{soft}} = & m_{H_d}^2 H_d^* H_d + m_{H_u}^2 H_u^* H_u + m_S^2 S^* S \\ & - \left(\epsilon_{ij} \lambda A_\lambda S H_d^i H_u^j + \frac{1}{3} \kappa A_\kappa S^3 + h.c. \right), \end{aligned} \quad (4)$$

where m_{H_d}, m_{H_u} and m_S are the soft breaking Higgs masses, with A_λ and A_κ being trilinear soft-breaking terms. Consequently, despite that in this model the usual MSSM bilinear μ -term is absent from the superpotential Eq. (3), which only possesses dimensionless trilinear couplings, when the scalar component of S acquires a VEV, $s = \langle S \rangle$, an effective interaction $\mu_{\text{eff}} H_d H_u$ is generated, with the effective parameter $\mu_{\text{eff}} = \lambda s$, which is then naturally of the EW scale [34].

In addition to terms from $\mathcal{L}_{\text{soft}}$, the tree-level scalar Higgs potential receives the usual D and F term contributions:

$$\begin{aligned} V_D = & \frac{g_1^2 + g_2^2}{8} (|H_d|^2 - |H_u|^2)^2 + \frac{g_2^2}{2} |H_d^\dagger H_u|^2, \\ V_F = & |\lambda|^2 (|H_d|^2 |S|^2 + |H_u|^2 |S|^2 + |\epsilon_{ij} H_d^i H_u^j|^2) + |\kappa|^2 |S|^4 \\ & - (\epsilon_{ij} \lambda \kappa^* H_d^i H_u^j S^{*2} + h.c.), \end{aligned} \quad (5)$$

where g_1 is the gauge coupling of the electroweak $SU(2)_L$ and g_2 is the gauge coupling of the $U(1)_Y$ of the SM. Using the minimization conditions derived for the Higgs VEVs, one can re-express the soft breaking Higgs masses in terms of λ , κ , A_λ , A_κ , $v_d = \langle H_d^0 \rangle$, $v_u = \langle H_u^0 \rangle$, and s :

$$\begin{aligned} m_{H_d}^2 = & -\lambda^2 (s^2 + v^2 \sin^2 \beta) - \frac{1}{2} M_Z^2 \cos 2\beta + \lambda s \tan \beta (\kappa s + A_\lambda), \\ m_{H_u}^2 = & -\lambda^2 (s^2 + v^2 \cos^2 \beta) + \frac{1}{2} M_Z^2 \cos 2\beta + \lambda s \cot \beta (\kappa s + A_\lambda), \\ m_S^2 = & -\lambda^2 v^2 - 2\kappa^2 s^2 + \lambda \kappa v^2 \sin 2\beta + \frac{\lambda A_\lambda v^2}{2s} \sin 2\beta - \kappa A_\kappa s, \end{aligned} \quad (6)$$

where $v^2 = v_1^2 + v_2^2 = 2M_W^2/g_2^2$, and M_W is the mass of the W-boson.

Consequently, at the EW scale, the free parameters in the Higgs sector (at tree level) are: $\lambda, \kappa, m_{H_1}^2, m_{H_2}^2, m_S^2, A_\lambda$ and A_κ . Using the fore-mentioned minimization conditions of the Higgs potential, one can eliminate the soft Higgs masses in favour of $M_Z, \tan\beta$ and μ , resulting in $\lambda, \kappa, \tan\beta, \mu, A_\lambda, A_\kappa$ as a set of independent parameters. In our scans we will actually use a somewhat different set of parameters, including the soft scalar masses as well as the soft gaugino masses, M_1, M_2 and M_3 which are all free parameters at the EW scale; these parameters will all be listed in Sec. IV B.

B. Results

In this subsection we present the results of our scan of the NMSSM which were obtained as described in Sec. II. In Sec. III, we observed that, in the MSSM, even without imposing gaugino unification, the constraints on the Higgs sector from LEP and the Tevatron were significant in reducing the number of scan points possessing small values of m_χ that also yielded a relic density within 2σ of the experimental best-fit value.

Analogous to our scan over MSSM parameters, in order to evade LEP bounds on the chargino mass for our scan of the NMSSM, we again relax the assumption of universality amongst the gaugino masses: M_1, M_2 and M_3 at the unification scale. Consequently, we allow the bino mass to be very small without the implication of yielding an unacceptably light chargino. Further, we must also satisfy LEP constraints on the invisible Z width. Because of the gaugino non-universality, the majority of the points selected in our MSSM scan were bino-dominated with a gaugino fraction $g_f > 0.6$. Similarly, the dominant bino composition of our points selected in our NMSSM scan helps evading the constraint on Γ_Z , which is proportional to the difference between the squares of the higgsino components of the neutralino LSP [15].

Alternatively, in the NMSSM, one can potentially evade the collider constraints with the neutralino LSP that possesses a dominant singlino contribution. Then bino-dominated neutralinos, bino/singlino mixed neutralinos and singlino-like neutralinos are possible as a light LSP [36]. In these three scenarios, for neutralino masses below ~ 15 GeV, efficient annihilation is achieved mainly via a light Higgs resonance exchange [37]. Therefore, in order to obtain an acceptable range of the relic density for a very light neutralino, one needs in general very light Higgses with the mass of the lightest Higgs scalar m_{h_1} tuned to be close to $2m_\chi$. This implies that, in order to evade LEP bounds, the lightest Higgs must be singlet-like. In order to generate this kind of Higgs boson without driving down the mass of the SM Higgs below the LEP bound of $\simeq 114.4$ GeV [28], one needs to decouple the singlet and doublet Higgs components (i.e., obtain the limit $\mathcal{M}_{S,13}^2, \mathcal{M}_{S,23}^2 \rightarrow 0$ for the mass matrix \mathcal{M}_S of CP-even Higgs states (see, e.g., Eq. (2.8) of [38])).

As discussed in [39], there are two possible ways to achieve this. One is to adopt the limit $\lambda \rightarrow 0$. Alternatively, one can enforce the relation:

$$A_\lambda = \frac{2}{\sin 2\beta} \mu_{\text{eff}} - 2\kappa s. \quad (7)$$

Adopting Eq. (7) exactly yields a mass for the lightest CP-even singlet Higgs scalar given by

$$m_{h_1}^2 = \lambda^2 A_\lambda \frac{v_1 v_2}{\lambda s} + \kappa s (A_\kappa + 4\kappa s), \quad (8)$$

which is equal to $M_{S,33}^2$ (once again, see, e.g., Eq. (2.8) of [38]). Such solutions were found in the study conducted by Bélanger *et al.* [37]. From Eq. (8), we can see that there are new types of solutions present in the NMSSM that are not obtainable in the MSSM. In the limit $\lambda \rightarrow 0$, the mass of the CP-odd neutral scalar Higgs (i.e., the pseudoscalar Higgs) is given by

$$m_{\text{pseudoscalar}}^2 = \lambda \left(2\kappa + \frac{A_\lambda}{2s} \right) v^2 \sin 2\beta - 3\kappa A_\kappa s \rightarrow -3\kappa A_\kappa s, \quad (9)$$

which is equal to $\mathcal{M}_{P,22}^2$, where \mathcal{M}_P is the mass matrix of CP-odd Higgs states, and where, in the limit $\lambda \rightarrow 0$, $\mathcal{M}_{P,12} \rightarrow 0$ and hence, due to the zero mass terms of the Goldstone boson, \mathcal{M}_P is diagonal (see, e.g., Eq. (2.10) of [38]). From Eq. (9) we can see that a negative value of $\kappa A_\kappa s$ is necessary in order to obtain $m_{\text{pseudoscalar}}^2 > 0$ and, consequently, avoid tachyons ². For small λ it will be difficult to achieve a resonance annihilation via a singlet Higgs

² Notice that without loss of generality λ can be chosen to be positive [38] and that with this convention the sign of s and the sign of μ_{eff} are the same.

Parameter	Range	Parameter	Range
bino mass	$0.1 < M_1 < 30$	CP-odd neutral scalar Higgs mass	$85 < m_A < 600$
wino mass	$90 < M_2 < 500$	slepton-left mass	$70 < m_{\tilde{L}} < 3000$
μ_{eff} parameter	$90 < \mu_{\text{eff}} < 500$	slepton-right mass	$70 < m_{\tilde{R}} < 3000$
ratio of Higgs doublet s	$2 < \tan \beta < 65$	trilinear terms	$ A_\kappa < 100, \tilde{A} < 4000$
Higgs sector coupling	$10^{-4} < \lambda < 0.5$	Higgs sector coupling	$10^{-4} < \kappa < 0.5$

TABLE III. The prior ranges of input parameters over which we perform our scan of the NMSSM. All displayed mass ranges are given in GeV. We adopt log priors for all input parameters except $\tan \beta$, for which we use a flat prior.

when the neutralino is singlino-like due to tendency for the masses of the neutralino LSP and the Higgs to be similar. Hence, in this case, a bino-dominated neutralino LSP will be favoured.

Conversely, for larger λ , it is possible to generate nearly pure singlet-like Higgs states by fine-tuning A_λ according to Eq. (7). These solutions allow for singlino-like neutralinos that annihilate via a singlet-like Higgs that are much more efficient than those corresponding annihilations involving a bino-like LSP. Since the constraints from LEP on the chargino mass ultimately yields a lower bound on $\mu_{\text{eff}} = \lambda s$, and from Eq. (7), a hierarchy is established between λ and κ , where $\kappa \ll \lambda$ for $\lambda \gg 0$, in such a way as to result in a small value of $m_\chi \sim 2\kappa s$. Alternatively, for large λ , one may avoid this hierarchy as well as generate a light, pure, singlet-like CP-even or CP-odd Higgs by finely-tuning A_κ to drive down the mass given by Eq. (8) or Eq. (9) respectively. Such fine-tuning allows for LSPs similar to those found in [20]. As a result of these two fine-tuning scenarios, the solutions in the regime $\lambda > 0.1$ are generally finely-tuned, resulting in mixed bino-singlino LSPs.

Taking into account all our constraints (i.e., DM relic density, collider and flavour physics), one can determine that

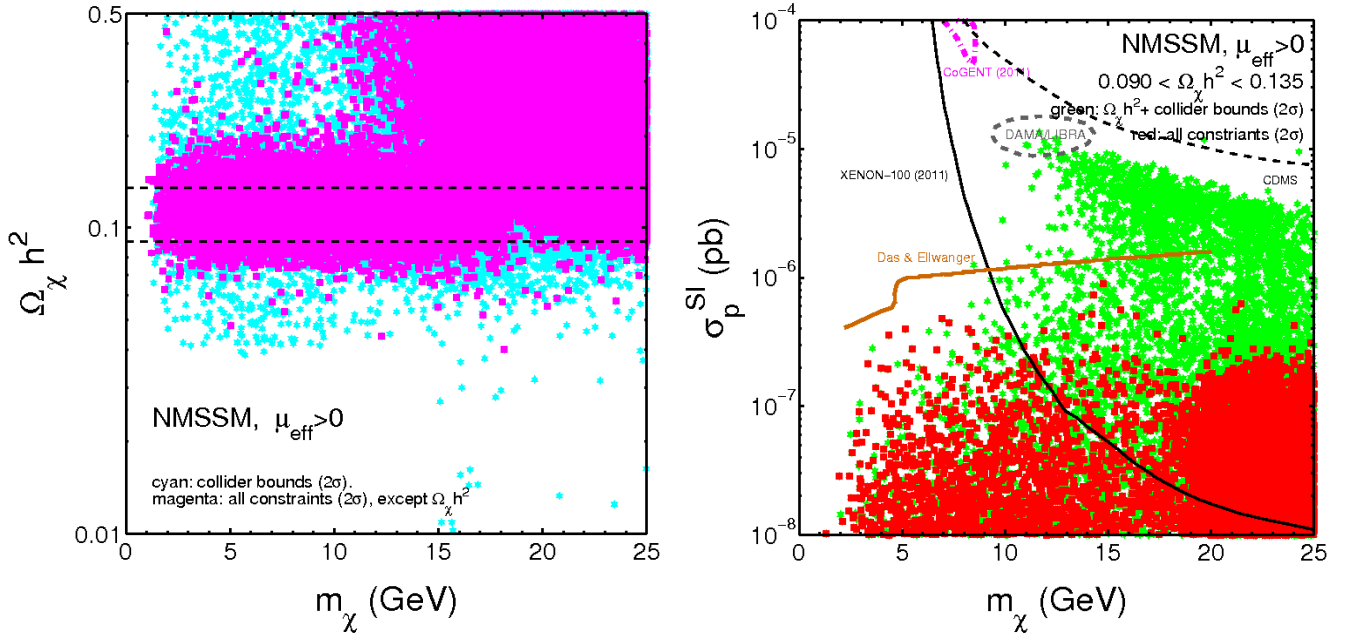


FIG. 3. *Left panel:* m_χ vs. $\Omega_\chi h^2$ in the NMSSM. Cyan points: all the points resulting from our NS scan, where constraints on $\Omega_\chi h^2$ and flavour physics bounds are included in the likelihood as Gaussians, and collider constraints are included in the likelihood as hard cuts. All relevant constraints are specified in Table I. Magenta points: points from our initial scan surviving subsequent 2σ hard cuts using flavour physics constraints. We also indicate the 2σ range of relic densities within the experimental best-fit value (black dashed curves). *Right panel:* m_χ vs. σ_p^{SI} in the NMSSM. Green points: those of the cyan points in the left panel which survive a subsequent 2σ hard cut on $\Omega_\chi h^2$. Red points: those of the magenta points in the left panel that survive a subsequent 2σ hard cut on $\Omega_\chi h^2$. We also illustrate the regions of parameter space currently favoured by CoGENT (outlined by the magenta dash-dotted curve), DAMA/LIBRA (with ion channelling, outlined by the dashed grey curve), and illustrate the current limits from CDMS-II (dashed black curve) and XENON-100 (solid black curve). We also display the estimated upper bound on σ_p^{SI} in the NMSSM according to Das & Ellwanger [17] when using default values of strange quark content in nucleons (orange curve).

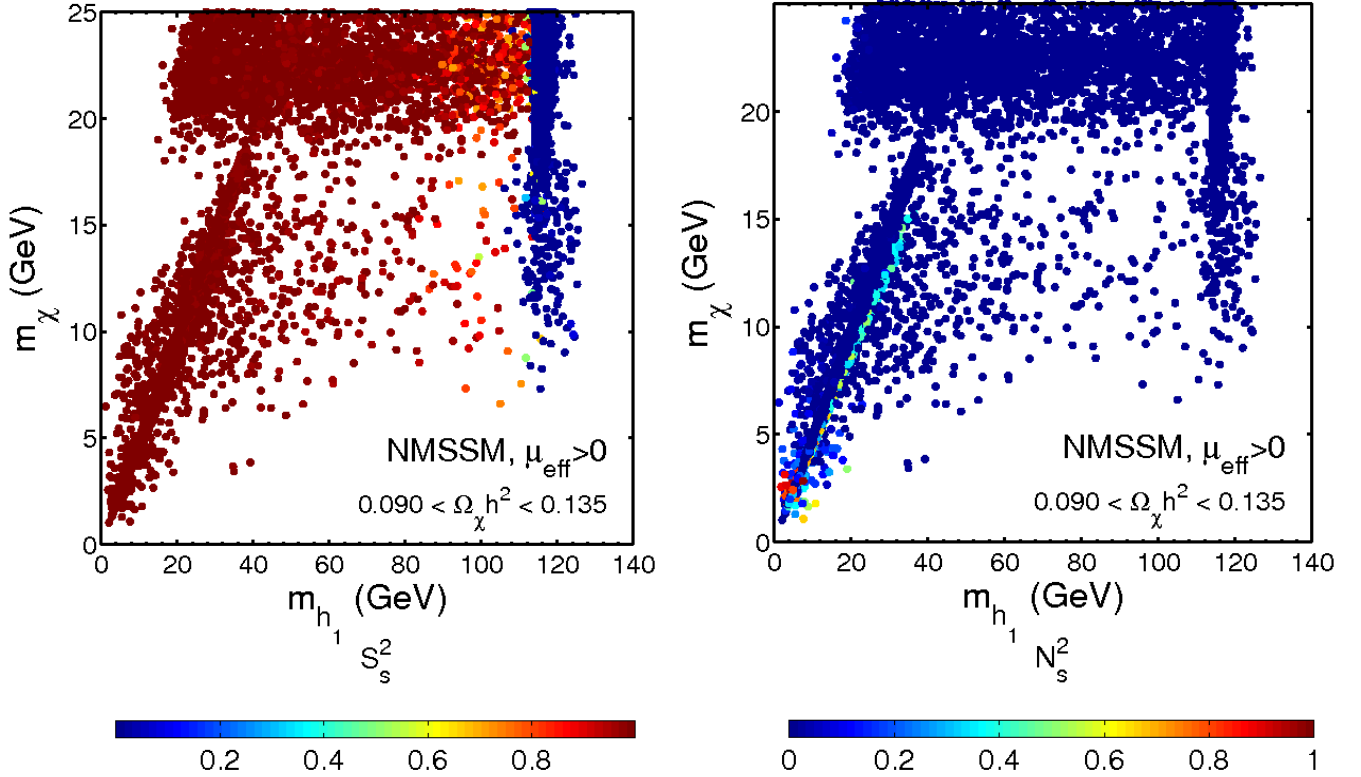


FIG. 4. *Left panel:* m_{h_1} vs. m_{χ} in the NMSSM, for the points from our initial NS scan that survive subsequent 2σ hard cuts on $\Omega_{\chi} h^2$ and when using constraints from colliders (including flavour physics). The colour scale illustrates the singlet fraction S_s^2 of the lightest Higgs. *Right panel:* Identical to the left panel except now the colour scale indicates the singlino fraction of each respective neutralino LSP.

a value of $\lambda \sim 10^{-2}$ favours a bino-dominated neutralino LSP. For larger values of $\lambda \sim 10^{-1}$ neutralinos are a mixture of both bino and singlino. For this reason, the selection of either a log or flat prior for λ can make a huge difference to numerical results. We highlight the caveat that all such solutions are fine-tuned since $2m_{\chi} \approx m_{h_1}$ or $2m_{\chi} \approx m_{a_1}$, where m_{a_1} is the mass of the lightest doublet-like pseudoscalar Higgs (whereas the heavier doublet-like pseudoscalar mass is denoted by m_{a_2}), however for $\lambda \gtrsim 10^{-1}$ we find that a further numerical fine-tuning, this time involving A_{λ} , is necessary in order to generate a singlet Higgs pure enough to escape collider constraints. One should also mention that in this scenario collider constraints on the heavier, MSSM-like, CP-even Higgs h_2 become extremely important, favouring small values for $\tan \beta \sim 3$ [37].

Bearing in mind the above, we performed our scan of the NMSSM, using the NMSPEC code [23] and imposing all relevant constraints in the likelihood as described in Sec. II, taken over the following input parameters:

$$M_1, M_2, \mu_{\text{eff}}, m_A, m_{\tilde{L}_L}, m_{\tilde{L}_R}, A_{\kappa}, \tilde{A}, \tan \beta, \lambda, \kappa. \quad (10)$$

where m_A denotes the running mass of the lighter CP-odd Higgs-doublet, as defined in the NMSPEC code [23] (see Table III), and the other parameters in Eq. (10) have already been defined above³. where m_A is an approximative value for m_{a_1} . Once again, we adopt log priors for all input parameters except $\tan \beta$, for which we use a flat prior, when conducting our scans. In particular, we utilise a log prior for λ and κ so that we may explore the general behaviour of low mass LSPs in the λ - κ plane, rather than adopt flat priors and focus on finely-tuned solutions possessing $\lambda \gg 0$, as in, e.g., [37]. Also, for the same reasons as, and in order to be consistent, with our scan of the MSSM, we assume all slepton soft mass parameters as well as their right-handed partners to be degenerate and fix the gluino and all squark masses at 1 TeV. The prior ranges of the NMSSM parameters Eq. (10) over which our scan is performed are provided in Table III. In analogy to our MSSM scan, we restrict the bino mass to the range $0.1 \text{ GeV} < M_1 < 30 \text{ GeV}$ and the

³ Note that in the NMSPEC code, when m_A is chosen as input, A_{λ} is treated as output.

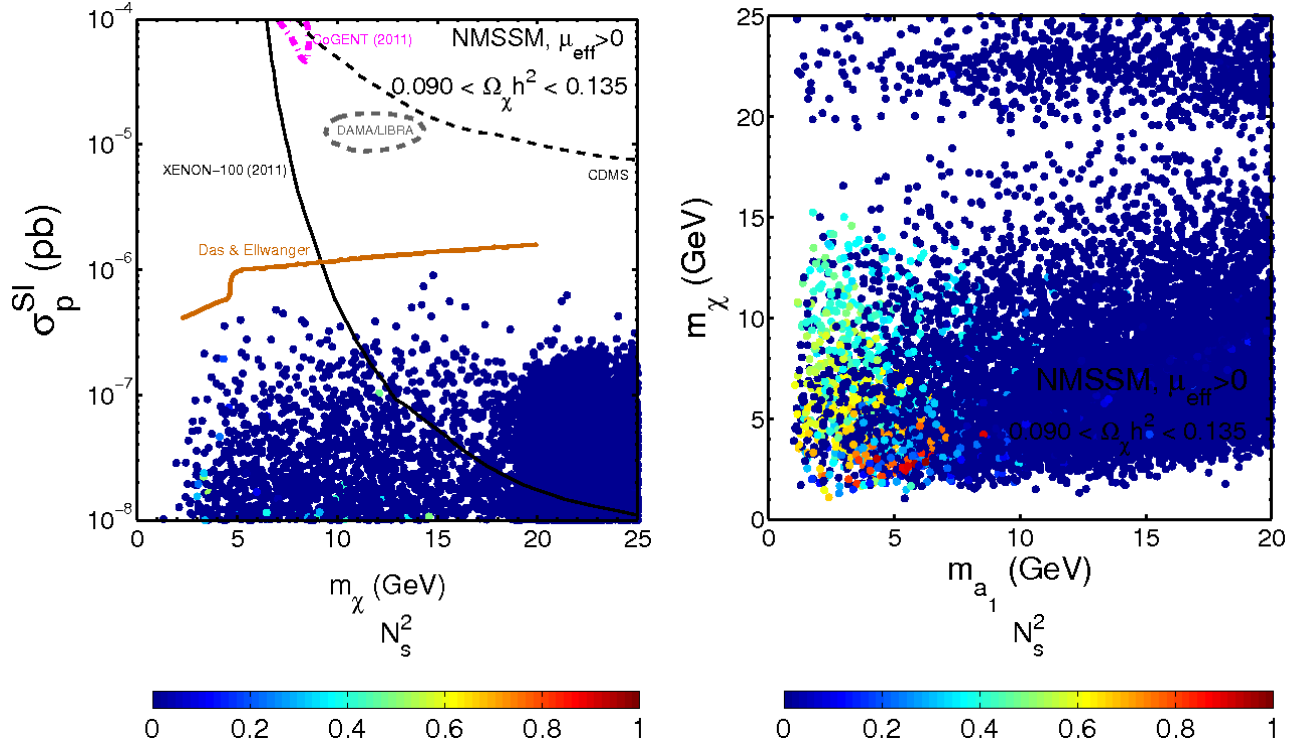


FIG. 5. *Left panel:* m_χ vs. σ_p^{SI} in the NMSSM, for the points from our initial NS scan that survive subsequent 2σ hard cuts on $\Omega_\chi h^2$ and when using constraints from colliders (including flavour physics). The colour scale indicates the singlino fraction of each respective neutralino LSP. The experimental bounds and theoretical limits are identical to those displayed in the right panel of Fig. 3. *Right panel:* m_{a_1} vs. m_χ in the NMSSM, using the same points as those displayed in the left panel.

higgsino mass parameter to the range $90 \text{ GeV} < \mu_{\text{eff}} < 150 \text{ GeV}$, in order to focus on light, bino-like neutralino LSP and evade collider constraints on the Higgs sector, as discussed above.

We present the results of our scan in the left panel of Fig. 3, displayed in the m_χ - $\Omega_\chi h^2$ plane. Cyan points correspond to those resulting from our initial scan, where collider constraints have been invoked in the relevant likelihood as hard cuts, differing from our MSSM scan, as described in Sec. II, but with the constraints on $\Omega_\chi h^2$ and those from flavour physics being invoked using a Gaussian assumption, as with our MSSM scan. The magenta points in the left-panel of Fig. 3 then correspond to those of the cyan points that survive a subsequent 2σ hard cut utilising flavour physics constraints. For both data sets, we observe that it is possible to generate points in the NMSSM that yield a relic density within 2σ of the experimental central value from WMAP, which are indicated by horizontal black dashed lines. However, as in the MSSM case, we can see many points where their associated relic density is many orders of magnitude larger than 0.1, due to premature thermal freeze-out brought about by the insufficient annihilation rates of the respective LSP cases.

In the right panel of Fig. 3, we demonstrate the effect of applying our different hard cuts on the m_χ - σ_p^{SI} plane. The light green and red points correspond to those points that survive respective 2σ hard cuts on $\Omega_\chi h^2$ on the cyan and magenta points displayed in the left panel of Fig. 3. For comparison, we also superimpose current limits from CoGENT, DAMA/LIBRA (with ion channelling), CDMS-II and XENON-100. We observe that the majority of our selected points typically generate values of the SI elastic scattering cross section in the range $\sigma_p^{SI} \lesssim 10^{-7} \text{ pb}$. We also note that many of the green points generate much larger values of σ_p^{SI} , up to $2 \times 10^{-5} \text{ pb}$, however, the bino fraction of these neutralino LSPs are too small to survive our hard cuts involving flavour physics constraints.

From Fig. 3 (right panel) we also observe that our results, following our 2σ hard cuts, coincide well with the corresponding upper limits on σ_p^{SI} estimated by Das & Ellwanger [17] (orange curve) using their default model regarding the strange quark content of nucleons. Despite this agreement, we also note that the studies conducted by Vázquez *et al.* [18] and Cao *et al.* [20] generate results that include a small population of neutralino LSPs with σ_p^{SI} as large as 10^{-2} pb with $m_\chi \sim 10 \text{ GeV}$. We note that the σ_p^{SI} values of these points grossly violate the DD limits from XENON-100 by up to four orders of magnitude, as do the majority of the points we obtain possessing $\sigma_p^{SI} \gtrsim 10^{-6} \text{ pb}$,

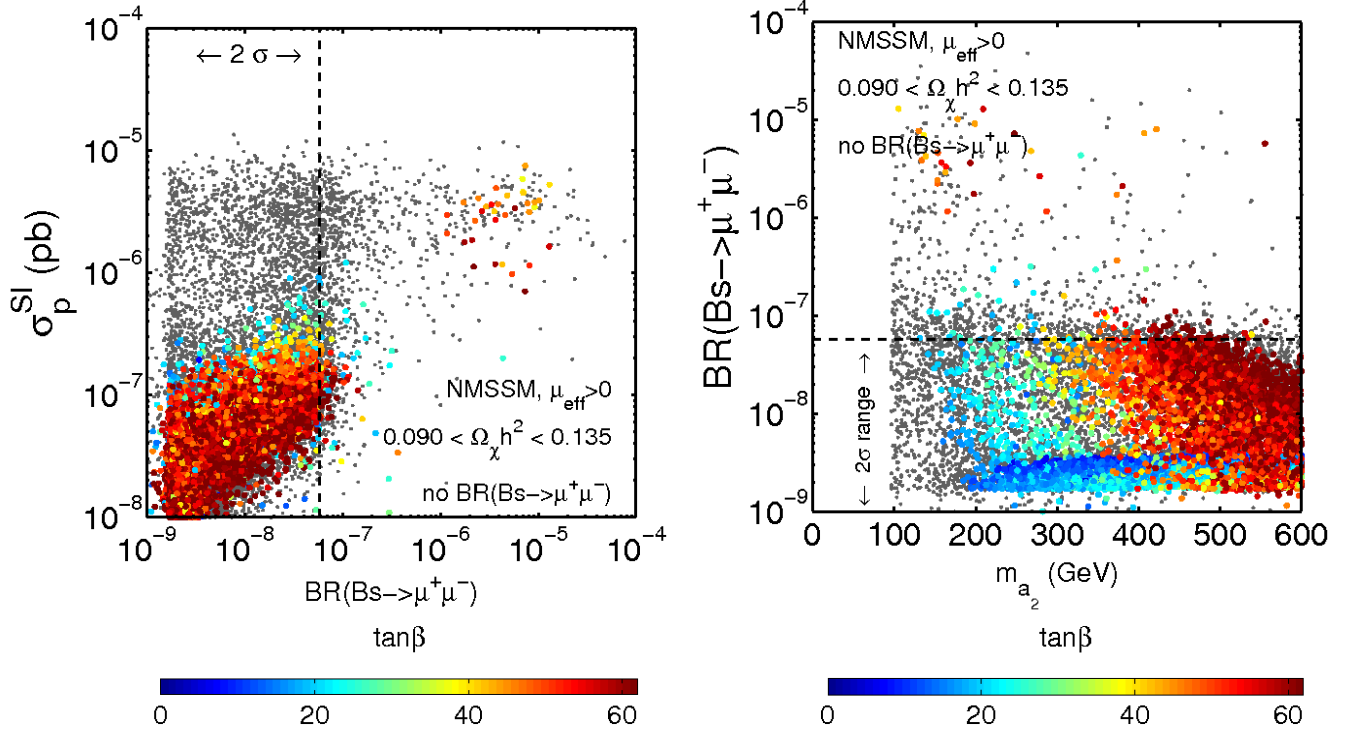


FIG. 6. *Left panel:* $BR(\overline{B}_s \rightarrow \mu^+ \mu^-)$ vs. σ_p^{SI} in the NMSSM. Grey points: points resulting from our initial NS scan that survive a subsequent 2σ hard cut on $\Omega_\chi h^2$. Coloured points: those of the grey points displayed which survive further 2σ hard cuts from colliders (including flavour physics constraints, except that relating to $BR(\overline{B}_s \rightarrow \mu^+ \mu^-)$). The colour scale displayed indicates the value of $\tan\beta$ associated with each neutralino LSP. *Right panel:* m_{a_2} vs. $BR(\overline{B}_s \rightarrow \mu^+ \mu^-)$ in the NMSSM, using the same points as displayed in the left panel.

and hence their omission do not effect our conclusions regarding the viable regions of NMSSM parameter space that are consistent with such current experimental limits. Moreover, we also remind the reader that, as described in Sec. II, we implicitly invoke our collider constraints as 2σ hard cuts during our scan of the NMSSM, and hence omit points that grossly violate such constraints.

In Fig. 4, we plot the respective values of m_{h_1} against m_χ , associated with the points from our initial scan surviving subsequent 2σ hard cuts using flavour physics constraints. We observe that, for $m_\chi \lesssim 15$ GeV, the reason why these points survive our hard cuts on $\Omega_\chi h^2$ is predominantly because of the existence of an s -channel resonance annihilation of the neutralino LSP via the lightest singlet-like Higgs, i.e., where $2m_\chi \simeq m_{h_1}$. This can be seen in the left panel of Fig. 4, where we plot the singlet fraction, S_s^2 , of the lightest Higgs as a third axis. The points corresponding to the LSP annihilating through the Higgs resonance also possess the lightest Higgs that is mostly singlet, which is essential in order to evade collider constraints on m_{h_1} . We also observe points with $m_\chi \gtrsim 15$ GeV that also survive our hard cuts on $\Omega_\chi h^2$. These points correspond to those configurations where one has very light slepton masses for all three generations, by virtue of our relaxation of the universality of slepton masses, allowing one to obtain a small enough relic density through additional t -channel annihilations, as is the case in the MSSM. For masses of the lightest Higgs in the range $m_{h_1} \gtrsim 114.4$ GeV we also observe the onset of the MSSM-like scenario, where the lightest Higgs is completely doublet-like, since we are now in the LEP-allowed region.

In Fig. 5 we display our results in the $m_\chi - \sigma_p^{\text{SI}}$ plane (left panel) and in the $m_{a_1} - m_\chi$ plane (right panel). In the left panel of Fig. 5, we can clearly see that there are only a minority of our selected points that possess a significant singlino component that survive our cuts and generate a value of $\sigma_p^{\text{SI}} > 10^{-7}$ pb. In the right panel of Fig. 5 we observe that for some surviving configurations the lightest pseudoscalar is lighter than the lightest neutralino. For these configurations, if the neutralino LSP also possesses a significant singlino component, annihilations where pseudoscalars are in the final state become significant. This explains the presence of those few singlino-dominated points in the right panel of Fig. 4, where we present the singlino fraction, N_s^2 , of the neutralino LSP of the points displayed in the left panel of Fig. 4 (via a colour scale), residing below those undergoing the resonance annihilations via the lightest scalar Higgs (i.e., $2m_\chi \simeq m_{h_1}$). Alternatively, there is the possibility of configurations possessing a neutralino LSP that undergoes a resonance annihilation via the pseudoscalar Higgs (i.e., $2m_\chi \simeq m_{a_1}$), which is also evident in Fig. 5. Such annihilation

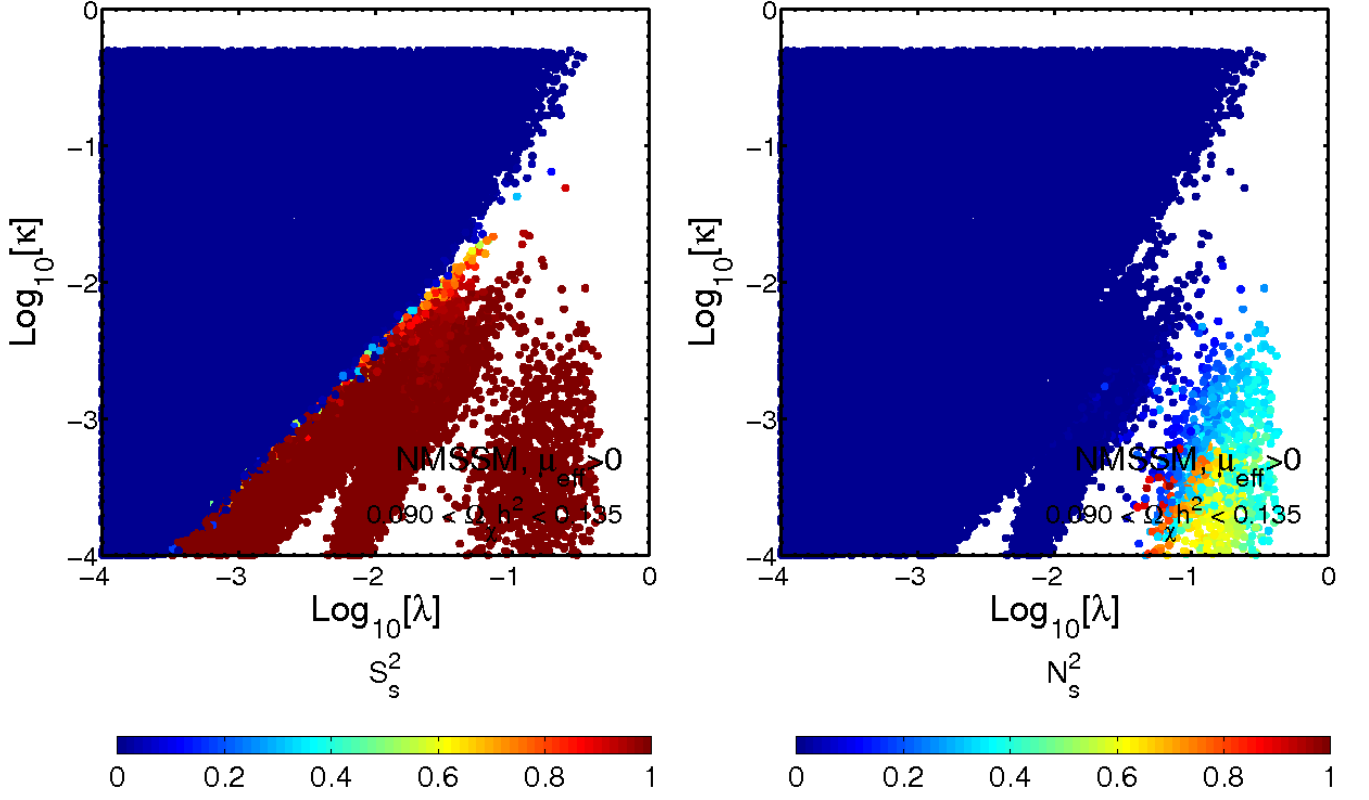


FIG. 7. *Left panel:* $\log_{10} \lambda$ vs. $\log_{10} \kappa$ in the NMSSM, for the points from our initial NS scan that survive subsequent 2σ hard cuts on $\Omega_\chi h^2$ and when using constraints from colliders (including flavour physics). The colour scale illustrates the singlet fraction S_s^2 of the lightest Higgs. *Right panel:* Identical to the left panel except now the colour scale indicates the singlino fraction of each respective neutralino LSP.

channels are evidently crucial in yielding an overall annihilation rate sufficiently large enough to generate the correct relic density (within the 2σ range) necessary to survive the invoked hard cuts.

The consequences of imposing the constraints from flavour physics are much more severe. This can be seen in Fig. 6, where the grey points represent those selected by our initial NS scan that survive a subsequent 2σ hard cut on $\Omega_\chi h^2$, and the coloured points represent those of the grey points that survive further 2σ hard cuts using flavour physics constraints except for that relating to $BR(\overline{B}_s \rightarrow \mu^+ \mu^-)$. In the left panel we display these points in the $BR(\overline{B}_s \rightarrow \mu^+ \mu^-) - \sigma_p^{\text{SI}}$ plane, and, in the right panel, the $m_{a_2} - BR(\overline{B}_s \rightarrow \mu^+ \mu^-)$ plane. In both plots we display the value of $\tan \beta$ associated with each configuration via a colour scale.

We observe that, like in the MSSM (see left panel of Fig. 2), configurations with large $\tan \beta$ typically yield a large SI elastic scattering cross section within the range $10^{-6} \text{ pb} \lesssim \sigma_p^{\text{SI}} \lesssim 10^{-5} \text{ pb}$, but are excluded by the constraint on $BR(\overline{B}_s \rightarrow \mu^+ \mu^-)$ from the Tevatron. In the right panel, we also observe a correlation between those points possessing large values of $\tan \beta$ and small values of $m_{a_2} \lesssim 300 \text{ GeV}$ and those possessing large values of $BR(\overline{B}_s \rightarrow \mu^+ \mu^-)$, analogous to the correlation between $BR(\overline{B}_s \rightarrow \mu^+ \mu^-)$, m_A and $\tan \beta$ in the MSSM displayed in Fig. 2. However, in the NMSSM, this correlation is evidently much weaker than in the MSSM due to the additional degrees of freedom relating to the two pseudoscalar Higgs masses.

Finally, in Fig. 7 we present our results in the $\lambda - \kappa$ plane with third axes displaying the singlino composition of the lightest Higgs scalar (left panel) and singlet composition of the lightest Higgs (right panel). We clearly observe that our scan points are segregated into several different regions in the $\lambda - \kappa$ plane, each with a distinctive minimum value of $\log_{10} \lambda$, containing points that we can ascribe to one of approximately four different categories that we will now discuss.

Starting at small values of λ we observe the following categories of points: (i) At $\lambda \sim 10^{-4}$ we can see the onset of the MSSM-like region, consisting of bino-dominated LSPs with $m_\chi \gtrsim 7 \text{ GeV}$ (see left panel of Fig. 4), with the lightest Higgs scalar being doublet-like with $m_{h_1} \gtrsim 114.4 \text{ GeV}$ in order to evade LEP bounds. In this case the neutralino annihilates mainly through a t -channel slepton exchange as described earlier in this section. (ii) For $\lambda \sim 10^{-3}$ and

$\kappa \sim 10^{-4}$ we observe the onset of a region where $m_\chi \gtrsim 15$ GeV and, as with the MSSM-like region, the LSP is bino-dominated and still annihilates mainly via t -channel slepton exchange, but in this case the lightest Higgs is singlet-like. (iii) For $\lambda \sim 10^{-2}$ we find the onset of those points involving bino-dominated neutralino LSPs that annihilate through the fore-mentioned s -channel resonance involving a singlet-like Higgs, possessing a mass following the relation: $m_\chi \approx 2m_{h_1}$. iv) Lastly, for $\lambda \gtrsim 10^{-1}$ we find neutralinos with $m_\chi \lesssim 15$ GeV which are now a mixture of both singlino and bino and, as with (iii), annihilate via a resonance involving a singlet-like Higgs. As explained in Sec. IV B, a degree of fine-tuning in A_λ , via Eq. (7), or in A_κ , via Eq. (9), is necessary in order to generate very light singlet-like Higgses for large values of $\lambda \sim 1$. Such solutions can potentially generate large values of the SI elastic scattering cross section that are several orders of magnitude larger than that associated with the bino-dominated case, for $\lambda \sim 10^{-2}$, depending on the degree of fine-tuning involved. However, as remarked earlier in this section, such points are clearly excluded by the DD limits, particularly those from XENON-100.

V. SUMMARY

In this paper we have re-examined the low mass neutralino region of both MSSM and NMSSM parameter space in light of the recent re-confirmation of a low energy excess of events observed by CoGENT, and the recent limits arising from the non-observations by XENON-100 that are in contention with the CoGENT data. To conduct our investigation we utilised focused NS scans when imposing a variety of experimental constraints, associated with (i) the cosmological DM relic abundance, (ii) direct collider search limits and (ii) collider physics relating to flavour physics and $\delta(g-2)_\mu$, in the likelihood. Unlike the majority of previous studies we then re-invoked each of these constraints on the resulting scan data, this time, via a successive series of 2σ hard cuts.

Firstly, regarding the MSSM, we relaxed the unification of gaugino masses in order to efficiently generate light, bino-like neutralino LSPs without violating collider constraints involving the invisible Z width and the chargino mass. We observed that for many configurations from our initial scan producing the neutralino LSP mass $m_\chi \gtrsim 5$ GeV the corresponding values of $\Omega_\chi h^2$ were small enough to be within the WMAP 2σ range. This could be achieved predominantly through efficient t -channel annihilations via stau exchange, which are enhanced for points possessing large $\tan\beta$. However, owing to LEP constraints on the slepton masses, when we invoked collider constraints as 2σ hard cuts, only bino-like LSPs with $m_\chi \gtrsim 11$ GeV survived. Moreover, when invoking the constraints from flavour physics, the minimum LSP mass was further increased to approximately $m_\chi \gtrsim 13$ GeV, which is slightly heavier than the values within the favoured CoGENT region, and much lighter than the 28 GeV limit claimed by Vasquez *et al.* [18]. We find that for these points it is extremely difficult to generate values of the SI elastic scattering cross section much larger than 10^{-5} pb, owing primarily to the constraints on the χHp coupling, which is enhanced for large $\tan\beta$, coming from flavour physics, particularly the limit on $BR(\bar{B}_s \rightarrow \mu^+\mu^-)$. We emphasise that this limit is particularly stringent within the framework of minimal flavour violation which we have adopted but can be fairly easily relaxed when one abandons it; see [40, 41]. However, we point out that solutions possessing such large values of σ_p^{SI} , within our permitted mass range of $m_\chi \gtrsim 13$ GeV, are also clearly excluded by the DD limits from XENON-100.

Regarding the NMSSM, once again, we conducted a focused NS scan in the low LSP mass region, where (non-flavour) collider constraints were invoked in the likelihood this time as 2σ hard cuts. Once again, in order to efficiently generate light neutralino LSPs without violating LEP bounds on the invisible Z width and the chargino mass, gaugino unification was relaxed. Whilst the majority of points surviving collider constraints were found to be bino-like, we found that a significant proportion of these points also evaded collider constraints by adopting a partial singlino component, made possible through the extended Higgs sector of the NMSSM. In such cases, we found that for light LSPs possessing $m_\chi \lesssim 15$ GeV we were able to generate values of $\Omega_\chi h^2$ small enough to lie within the WMAP 2σ range through s -channel resonance annihilations via the lightest CP-even Higgs. Consequently, in order to evade LEP bounds, in such cases the lightest Higgs had to be singlet-like, very much decoupled from the doublet Higgs. This could be achieved by adopting the limit $\lambda \rightarrow 0$, in which case bino-dominated LSPs are favoured, or by finely-tuning A_λ , generally resulting in a combination of bino-singlino LSP configurations and a hierarchy between λ and κ where $\kappa \ll \lambda$ for $\lambda \gg 0$ that we explicitly described, or by finely-tuning A_κ . However, for $m_\chi \gtrsim 15$ GeV, we found that points can generate $\Omega_\chi h^2$ small enough to survive our cuts by virtue of additional t -channel annihilations via very light sleptons, possible through our relaxation of the universality of slepton masses, or in some cases through s -channel annihilations via the pseudoscalar Higgs. We found that the points from our initial scan generated values of σ_p^{SI} up to approximately 2×10^{-5} pb. However, we found that many of these points possessed too large a bino fraction to survive the flavour physics constraints, particularly that coming from $BR(\bar{B}_s \rightarrow \mu^+\mu^-)$, that we later re-invoked as 2σ hard cuts, finding results very similar to those obtained in [17] where $\sigma_p^{\text{SI}} \lesssim 10^{-6}$ pb. We also highlight that many of these points with $m_\chi \gtrsim 10$ GeV are excluded by DD limits from XENON-100, like many of the points discussed by other authors, including [18, 20], that possess σ_p^{SI} as large as 10^{-2} pb, but are generated without invoking experimental

constraints as 2σ hard cuts, as we do, in order to omit points that grossly violate individual constraints.

ACKNOWLEDGMENTS

We would like to thank J. I. Collar and V. Kudryavtsev for their helpful comments regarding the CoGENT experiment and data analysis, and also to T. Varley for his participation early in the project. DTC is supported by the Science Technology and Facilities Council. DEL-F is supported by the French ANR TAPDMS ANR-09-JCJC-0146 and would like to thank the Science Technology and Facilities Council for its support at an earlier stage of this project. LR is funded in part by the Foundation for Polish Science and by the EC 6th Framework Programme MRTN-CT-2006-035505. R. RdA would like to thank the support of the Spanish MICINN's Consolider-Ingenio 2010 Programme under the grant MULTIDARK CSD2209-00064.

-
- [1] <http://cogent.pnnl.gov/>
 - [2] C. E. Aalseth *et al.* [CoGeNT collaboration], Phys. Rev. Lett. **106** (2011) 131301 [arXiv:1002.4703 [astro-ph.CO]].
 - [3] C. E. Aalseth *et al.*, arXiv:1106.0650 [astro-ph.CO].
 - [4] <http://people.roma2.infn.it/~dama/web/home.htm>
 - [5] R. Bernabei *et al.*, arXiv:1002.1028 [astro-ph.GA].
 - [6] F. Petriello and K. M. Zurek, JHEP **0809**, 047 (2008) [arXiv:0806.3989 [hep-ph]].
 - [7] S. Chang, A. Pierce and N. Weiner, Phys. Rev. D **79**, 115011 (2009) [arXiv:0808.0196 [hep-ph]].
 - [8] M. Fairbairn and T. Schwetz, JCAP **0901**, 037 (2009) [arXiv:0808.0704 [hep-ph]].
 - [9] C. Savage, G. Gelmini, P. Gondolo and K. Freese, JCAP **0904**, 010 (2009) [arXiv:0808.3607 [astro-ph]].
 - [10] C. Savage, K. Freese, P. Gondolo and D. Spolyar, JCAP **0909**, 036 (2009) [arXiv:0901.2713 [astro-ph]].
 - [11] <http://xenon.astro.columbia.edu/>
 - [12] E. Aprile *et al.* [XENON100 Collaboration], arXiv:1104.2549 [astro-ph.CO].
 - [13] <http://cdms.berkeley.edu/>
 - [14] Z. Ahmed *et al.* [The CDMS-II Collaboration], Science **327** (2010) 1619 [arXiv:0912.3592 [astro-ph.CO]].
 - [15] A. L. Fitzpatrick, D. Hooper and K. M. Zurek, Phys. Rev. D **81**, 115005 (2010) [arXiv:1003.0014 [hep-ph]].
 - [16] P. Draper, T. Liu, C. E. M. Wagner, L. T. M. Wang and H. Zhang, Phys. Rev. Lett. **106** (2011) 121805 [arXiv:1009.3963 [hep-ph]].
 - [17] D. Das and U. Ellwanger, JHEP **1009** (2010) 085 [arXiv:1007.1151 [hep-ph]].
 - [18] D. A. Vasquez, G. Belanger, C. Boehm, A. Pukhov and J. Silk, Phys. Rev. D **82** (2010) 115027 [arXiv:1009.4380 [hep-ph]].
 - [19] N. Fornengo, S. Scopel and A. Bottino, Phys. Rev. D **83** (2011) 015001 [arXiv:1011.4743 [hep-ph]].
 - [20] J. Cao, K. i. Hikasa, W. Wang and J. M. Yang, arXiv:1104.1754 [hep-ph].
 - [21] <http://projects.hepforge.org/multinest/>
 - [22] <http://superbayes.org/>
 - [23] U. Ellwanger and C. Hugonie, Comput. Phys. Commun. **177** (2007) 399 [arXiv:hep-ph/0612134]; <http://www.th.u-psud.fr/NMHDECAY/nmssmtools.html>
 - [24] N. Jarosik *et al.*, arXiv:1001.4744 [astro-ph.CO].
 - [25] E. Barberio *et al.* [Heavy Flavor Averaging Group (HFAG) Collaboration], arXiv:0704.3575 [hep-ex].
 - [26] D. Eriksson, F. Mahmoudi and O. Stal, JHEP **0811**, 035 (2008) [arXiv:0808.3551 [hep-ph]].
 - [27] K. Nakamura *et al.* (Particle Data Group), JPG **37**, 075021 (2010) (URL: <http://pdg.lbl.gov>)
 - [28] A. Sopczak, Nucl. Phys. Proc. Suppl. **109B**, 271 (2002) [arXiv:hep-ph/0112086].
 - [29] L. Roszkowski, R. Ruiz de Austri and R. Trotta, J. High Energy Phys. 07072007075.
 - [30] S. P. Martin, arXiv:hep-ph/9709356; H. E. Haber and G. L. Kane, Phys. Rept. **117**, 75 (1985).
 - [31] B. W. Lee and S. Weinberg, Phys. Rev. Lett. **39** (1977) 165.
 - [32] E. Lunghi, W. Porod and O. Vives, Phys. Rev. D **74**, 075003 (2006) [arXiv:hep-ph/0605177].
 - [33] C. Bobeth, T. Ewerth, F. Kruger and J. Urban, Phys. Rev. D **64**, 074014 (2001) [arXiv:hep-ph/0104284].
 - [34] U. Ellwanger, C. Hugonie and A. M. Teixeira, Phys. Rept. **496**, 1 (2010) [arXiv:0910.1785 [hep-ph]].
 - [35] J. E. Kim and H. P. Nilles, Phys. Lett. B **138** (1984) 150.
 - [36] J. F. Gunion, D. Hooper, B. McElrath, Phys. Rev. D **73** 015011 (2006) [arXiv:hep-ph/0509024].
 - [37] G. Belanger, F. Boudjema, C. Hugonie, A. Pukhov and A. Semenov, JCAP **0509**, 001 (2005) [arXiv:hep-ph/0505142].
 - [38] D. G. Cerdeño, C. Hugonie, D. E. López-Fogliani, C. Muñoz and A. M. Teixeira, J. High Energy Phys. 04122004048 [arXiv:hep-ph/0408102].
 - [39] U. Ellwanger and C. Hugonie, Mod. Phys. Lett. A **22**, 1581 (2007) [arXiv:hep-ph/0612133].
 - [40] J. Foster, K. i. Okumura and L. Roszkowski, JHEP **0508** (2005) 094 [arXiv:hep-ph/0506146]; J. Foster, K. i. Okumura and L. Roszkowski, JHEP **0603** (2006) 044 [arXiv:hep-ph/0510422].
 - [41] J. Foster, K. i. Okumura and L. Roszkowski, Phys. Lett. B **641** (2006) 452 [arXiv:hep-ph/0604121].